


RESEARCH ARTICLE | JANUARY 19 2024

Characterization and microstructure analysis of sodium alginate incorporate with iron (III) oxide for biomedical application

Wan Ahmad Mustaqim Ahmad Zakhi; Maizlinda Izwana Idris ; Nur Fatehah Mohd Nasir; Fateen Shamsaiha Hishamuddin



AIP Conf. Proc. 2925, 020047 (2024)

<https://doi.org/10.1063/5.0183205>



CrossMark

AIP Advances

Why Publish With Us?

-  **25 DAYS**
average time to 1st decision
-  **740+ DOWNLOADS**
average per article
-  **INCLUSIVE**
scope

[Learn More](#)

Characterization And Microstructure Analysis of Sodium Alginate Incorporate with Iron (III) Oxide for Biomedical Application

Wan Ahmad Mustaqim Ahmad Zakhi^{1, a)}, Maizlinda Izwana Idris^{1,2, b)}, Nur Fatehah Mohd Nasir^{1, c)} and Fateen Shamsaiha Hishamuddin^{1, d)}

¹*Faculty of Mechanical and Manufacturing Engineering, Universiti Tun Hussein Onn Malaysia, 86400, Parit Raja, Batu Pahat, Johor, Malaysia*

²*Bioactive Material Research Group (BioMa), Faculty of Mechanical and Manufacturing Engineering, Universiti Tun Hussein Onn Malaysia, 86400, Parit Raja, Batu Pahat, Johor, Malaysia*

^{a)} *wanmusaz@gmail.com*

^{b)} *Corresponding author: izwana@uthm.edu.my*

^{c)} *fatehahnasir17@gmail.com*

^{d)} *fateenshamsaiha@gmail.com*

Abstract. This research focuses on the characterisation of sodium alginate incorporated with Iron (III) oxide for biomedical applications. First, biofilm and bead samples with and without 0.1 g, 0.2 g, and 0.3 g iron (III)oxide particles are prepared by manual syringe technique and solution casting. Next, sodium alginate biofilms and beads incorporated with and without Iron (III) particles were analysed by microstructure using Scanning Electron Microscope (SEM). Energy–dispersive X-Ray Spectroscopy (EDS) analysis was applied as well to reveal the chemical elements present in the sample. The samples were characterised using X-Ray Diffraction (XRD) and Atomic Force Microscopy (AFM) analysis. Microstructure analysis results revealed that the microstructure of 0.1g, 0.2g, and 0.3g beads varied due to the amount of iron (III) oxide particles. Meanwhile, EDS detected that the chemical elemental present were mainly Fe^{3+} , O^{2-} , Ca^{2+} , and Cl^{-} . The existence of halite crystalline or sodium chloride, magnetite, sodium iron oxide, iron oxide, and maghemite structures was determined by XRD analysis to account for the varying diffraction peaks of the samples. Based on the AFM result, the surface roughness of all shapes resulted in different topography shapes due to the different weight of iron (iii) oxides that shows the increment of the weight resulted in the formation of different valleys and hills on the biofilm. Finally, the experiments concluded that sodium alginate incorporated with iron (III) oxide is promising for biomedical applications.

INTRODUCTION

Alginate is a naturally occurring polysaccharide from algae that have been widely studied and used for culinary and medical applications. Alginate is a naturally occurring anionic polymer that is typically derived from brown algae [1]. Sodium alginate (S.A.) is a remarkable natural polymer plentiful, biodegradable, hydrophilic, affordable, and easy to alter. Due to the abundant and easily modified carboxyl and hydroxyl groups on the molecule's backbone, S.A. was investigated to enhance the dye adsorption preference [2, 3]. The rate of drug release from hydrogels containing sodium alginate is relatively slow in a gastrointestinal environment. Alginate and alginate-based materials are extensively used in tissue engineering, wound dressings, drug delivery, dental impressions, transplantation, encapsulation, and cell therapy [4, 5]. Nevertheless, S.A. has limitations in the biomedical industry since it causes adverse gastrointestinal effects. As it is derived from alginic acid, it is acidic and, therefore, unsuitable for healthy diets. Its characteristics are poor mechanical strength and cell adhesion, low drug loading, hydrophilicity, microbial breakdown, and burst release. To overcome these concerns, S.A. has been mixed with a few synthetic and natural

polymers to improve its properties [3]. In the biomedical field, in terms of biopolymers, alginates are among the most used.

Nanoparticles of iron oxide have attracted the attention of a growing number of researchers because of their unusual properties of superparamagnetic, high magnetic susceptibility, low Curie temperature [6, 7] (in which the atoms of magnetic materials are aligned and parallel causing spontaneous magnetism), and no coercivity value. In terms of iron oxide nanoparticles, magnetite and maghemite are the most studied. Medication delivery, cell sorting, and magnetic fluid hyperthermia are a few of the many reported use for iron oxide nanoparticles today. Iron oxide nanoparticles are essential in magnetic resonance imaging (MRI) as well-known contrast agents [6]. Polymer matrix carrier selection and interactions or links with drug molecules in terms of physicochemical stability, targeting ability, drug loading, and release necessitated a careful study of magnetic nanoparticle functionalization. An iron-oxide polymer aids in the transport of particles across tissues. It is possible for these particles to be magnetized easily by an external magnetic field and to disperse immediately when the magnet is removed [8, 9].

As a result of technical breakthroughs, healthcare and therapeutics continue to evolve and progress. Biopolymers, mainly naturally produced, biocompatible, and biodegradable, are increasingly recognized as valuable in various therapeutic applications [4]. Biomedical applications such as magnetic resonance imaging for clinical diagnosis, magnetic medication targeting, hyperthermia as an anti-cancer strategy, and enzyme immobilization have piqued the interest of scientists in the production of biocompatible magnetic nanoparticles [10] for quite some time. One of the most exciting potential applications for magnetic nanoparticles is the targeted administration of medications [10]. Due to their biocompatibility, ease of surface modification, and magnetic properties, magnetic nanoparticles [11] have gained considerable interest in biomedical and industrial applications.

Numerous studies have been undertaken to exploit the considerable benefits of the distribution and controlled release of drug molecules, such as the capacity to target specific body parts and the reduction in the amount of medicine required for enhanced therapeutic efficacy with less severe side effects [12-22]. Once the carriers consisting of magnetic nanoparticles and drug molecules were concentrated at the target, the drug molecules were released by several situations, such as local physicochemical environment changes and applying an external magnetic field [20]. Thus, in this study experiments are carried out to conduct and investigate the microstructure analysis through Scanning Electron Microscope (SEM), to identify the chemical elements exist by using Energy Dispersive Spectroscopy (EDS), to observe and identify the crystallography of the particles by using X-Ray Diffraction analysis (XRD) and to identify the compatibility and the roughness by Atomic Force Microscopy (AFM) of the sodium alginate incorporated with iron (iii) oxide for biomedical applications.

MATERIALS AND METHODS

Sodium–alginate powder, Iron (III) oxide powder, and Calcium chloride dihydrate powder were obtained from Sigma Aldrich.

Preparation and Fabrication of Sodium Alginate Incorporate Iron (III) Oxides Biofilm

Alginate is added to 1000ml of distilled water at 1% (w/v). The S.A. solution is vigorously stirred with a magnetic stirrer before adding 0.1 g of Iron (III) oxide powder. When the iron (III) oxide is entirely disseminated with the alginate solution after 30 minutes in an ultrasonic vibration cleaning machine, the mixture is ready to be used. A 50 ml beaker is used to measure and transfer 25 ml of the mixture to a Petri plate. The S.A./iron (III) oxide combination is then allowed to settle for three days. 10 grammes of powdered calcium chloride dihydrate is weighed and added to 1000 ml of water after a three-day incubation period. A magnetic stirrer is used to agitate the calcium chloride for around 30 minutes. The solution is moved to a larger glass container. Three-day-old SA/iron (III) oxide samples are crosslinked in a calcium chloride solution. After that, the samples are allowed to dry for one day to create a biofilm. S.A. biofilm is made in the manner depicted in Figure 1.

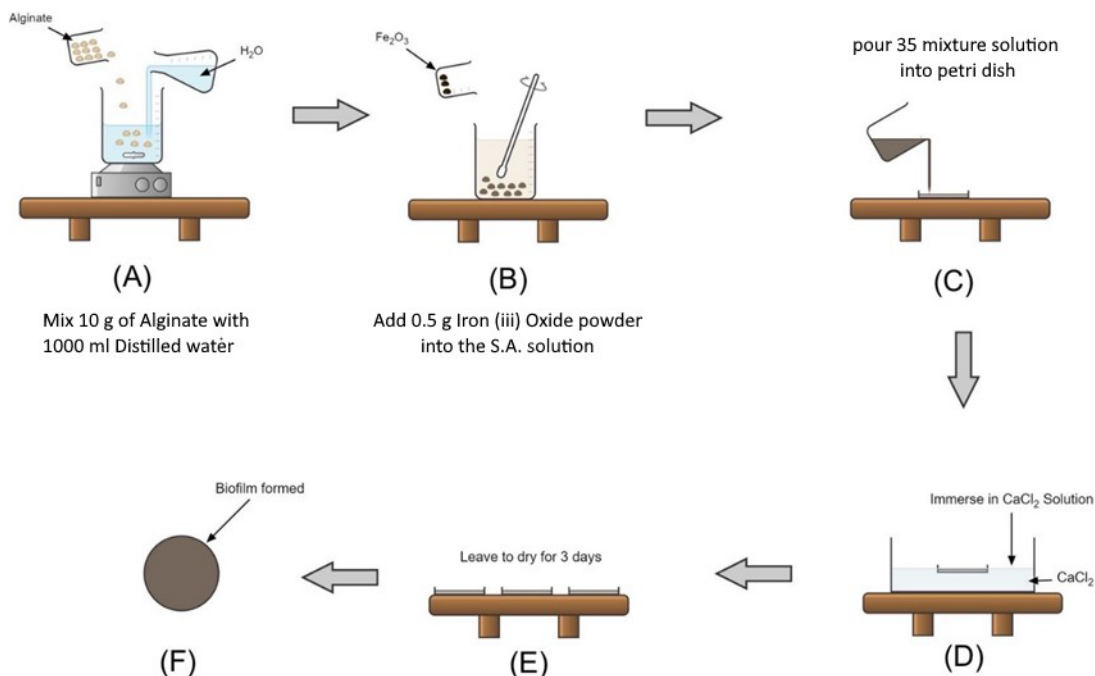


FIGURE 1. Schematic Diagram of Fabrication Process of S.A. + Iron (III) Oxides Biofilm.

Preparation and Fabrication of Sodium Alginate Incorporated Iron (III) Oxides Beads

Figure 2 depicts the fabrication procedure in action. It requires 1000ml of water and 1 per cent S.A. to make alginate/iron oxide beads. After vigorous stirring with a magnetic stirrer, 0.1 g of Iron (III) oxide powder is weighed and added to the S.A. solution. When the iron (III) oxide is entirely disseminated in the alginate solution, it is placed in an ultrasonic vibration cleaning machine for 30 minutes. The mixture is then injected into a 19 mm-diameter syringe with a volume of 20 ml to complete the procedure. A needle is used to eject the SA-iron (iii) oxide beads into a glass dish containing 20 ml of calcium chloride solution by applying pressure.

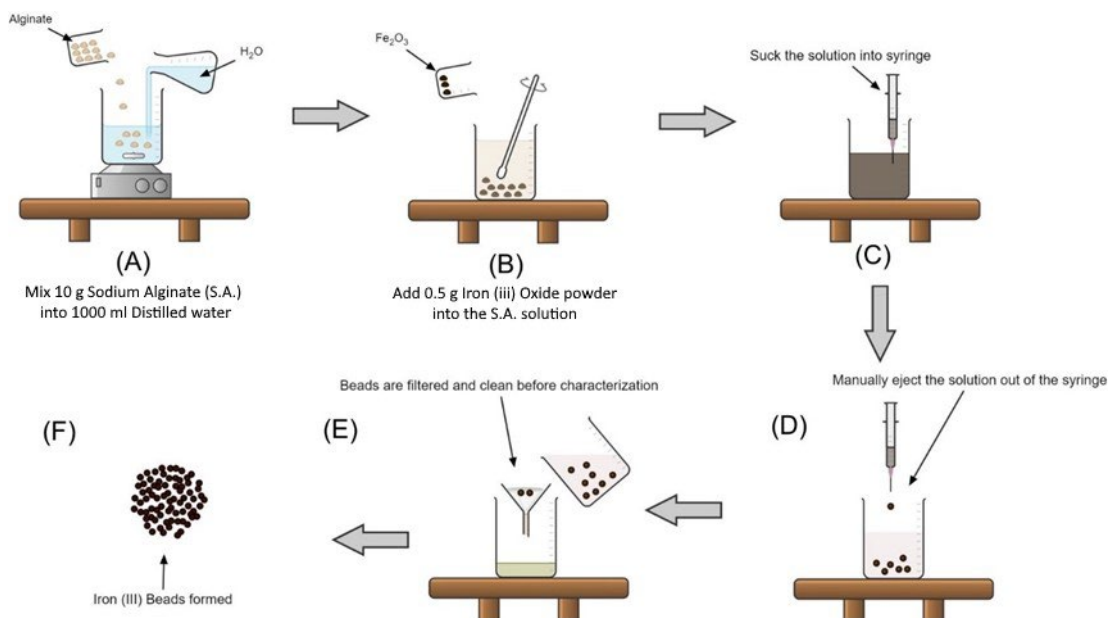


FIGURE 2. Schematic Diagram of Fabrication Process of S.A. + Iron (III) Oxides Beads.

Rinsing with distilled water is done after about ten minutes of soaking the beads in a calcium chloride solution. To keep their size and shape, the beads are left in a calcium chloride solution. The beads are removed and dried on filter paper before being characterized for characterization. Table 1 lists the composition factors utilized to create the biofilm and the beads in this experiment.

TABLE 1. Composition Parameters of S.A. 1% (w/v) with Iron (III) Oxide.

Sample Name	Iron (III) Oxide [g]
A	0.1
B	0.2
C	0.3

Characterization Of Sodium Alginate Incorporated Iron (III) Oxide Biofilm and Beads

Incorporating S.A. with iron (iii) oxides was tested using various characterization and analysis methods and procedures. SEM and EDS were analysed using biofilms and beads to assess the morphological structures and chemical components present. Biofilms were evaluated using a variety of characterizing approaches. S.A. containing Iron (iii) oxides biofilm was confirmed to have a crystalline structure using X-Ray Diffraction (XRD) at temperatures ranging from 20° to 90°. EVA software was used to evaluate the data after it was collected. AFM was used to determine the biofilm's surface roughness.

RESULTS AND DISCUSSIONS

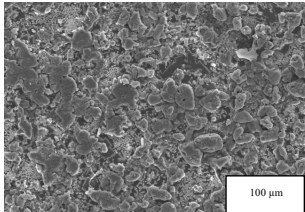
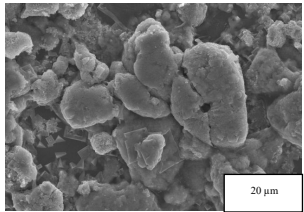
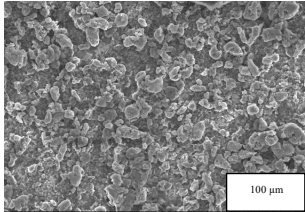
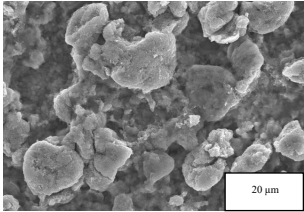
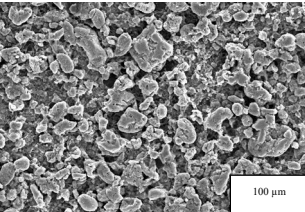
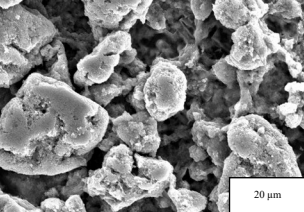
Scanning Electron Microscope (SEM) Analysis

The microstructure analysis of S.A. incorporated with Iron (III) Oxides was carried out by using both forms in biofilm and beads. Both biofilm and beads are coated beforehand. Table 2 shows the microstructure SEM images of S.A. 1% (w/v) incorporated with Iron (III) Oxides with three different parameters: 1 % (w/v) S.A. + 0.1 g Iron (III) Oxides [A], 1 % (w/v) S.A. + 0.2 g Iron (III) Oxides [B], and 1 % (w/v) S.A. + 0.3 g Iron (III) Oxides [C] at two different magnifications of 500x and 2000x. The SEM images of all three samples, A, B, and C, vary.

Low magnification of 500x shows microstructures with many grains distributed for all three samples – A, B, and C. High magnification of 2000x shows microstructures at a more focused area with a more porous surface of the microstructure of the iron oxides. At the higher magnification of 2000x, the microstructure and surface porosity of the iron oxides is more visible as the weight of the iron oxide increases. This is maybe due to the accumulation of iron oxide that is not dispersed evenly during the solution mixing, which then causes the biofilm formed has various visibility or presence of the iron oxide.

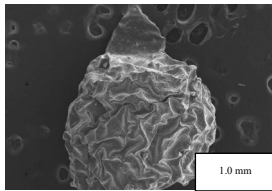
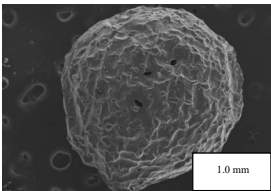
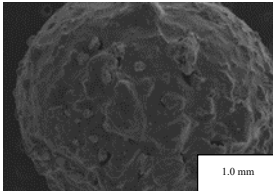
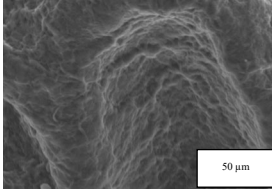
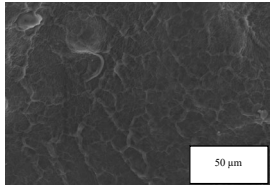
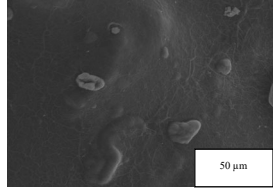
Table 2 shows SEM images of S.A. incorporating Iron Oxide Beads at two different magnifications; 500x and 2000x. A low magnification of 500x shows microstructures of the bead at a compact structure at a scale of 1.0 mm. The bead surface structure at 500x magnification for all three samples exhibits particle arrangement that looks like a more porous surface. High magnification of 2000x shows more detail and focused area of the bead's microstructures. At this higher magnification, the microstructure of the beads appears to be cloudier, like more wrinkled [23] and non-porous for both samples A and B, while sample C seems to be observed the presence of grains on the surface of the beads. Compared to the microstructure of biofilm for all three samples as depicted in Table 3, the bead's microstructure appears to be less porous and has almost no presence of grains which is the accumulation of iron oxide particle on the microstructure of the beads. Based on the microstructure images, it can be concluded that when the bead is form, not all iron and alginate are crosslinking and bonded with ion formation of the calcium chloride. Bead images of sample A seem to be more shrunken compared to samples B and C due to over exposure in the air after being taken out of the Calcium Chloride solution, which was able to help retain the spherical shape of the beads.

TABLE 2. Microstructure SEM Images of S.A. 1% (w/v) with Iron (III) Oxide Biofilm

Sample Name	500x magnification	2000x Magnification
1% (w/v) + 0.1 g (A)		
1% (w/v) + 0.2 g (B)		
1% (w/v) + 0.3 g (C)		

The preferable size for the beads must be in spherical shape as to allow a more biological distribution of particle or drug delivery into tissue vessels in human blood vessels and capillaries. A shrunken or non – spherical beads may have a larger particle accumulation on one side of the surface in which during the delivery may have interaction with vessels walls [24]. Sample C in biofilm formed, which is illustrated in Table 2 has the better microstructure images compared to all the other samples A and B in Table 2 and in comparison, with the microstructure images of all samples in beads form which is illustrated in Table 3.

TABLE 3. Microstructure SEM Images of S.A. 1% (w/v) with Iron (III) Oxide Beads

Sample Name	1% (w/v) + 0.1 g (A)	1% (w/v) + 0.2 g (B)	1% (w/v) + 0.3 g (C)
50x magnification			
1000x Magnification			

Energy Dispersive X – Ray Spectroscopy (EDS) Analysis

EDS Elemental analysis was carried out concurrently with the samples analysed of the microstructure analysis. The graphs for samples A, B and C in both Figure 3 and Figure 4 vary with each other. Elemental composition for both biofilm and beads for samples A, B, and C vary. In Table 4, chemical elemental analysis finds more elements in the biofilm compared to elements found in beads which are tabulated in Table 5. Chemical elemental analysis on the biofilm found more elements such as Fe^{2+} , O^{2-} , Na^+ , Ca^{2+} , and Cl^- , which in all three samples, A, B and C, have a high weight percentage of Iron. The presence of these elements could be due to the ionic interactions of the S.A./Iron (III) Oxides with Calcium Chloride solutions while crosslinking to form a biofilm shape.

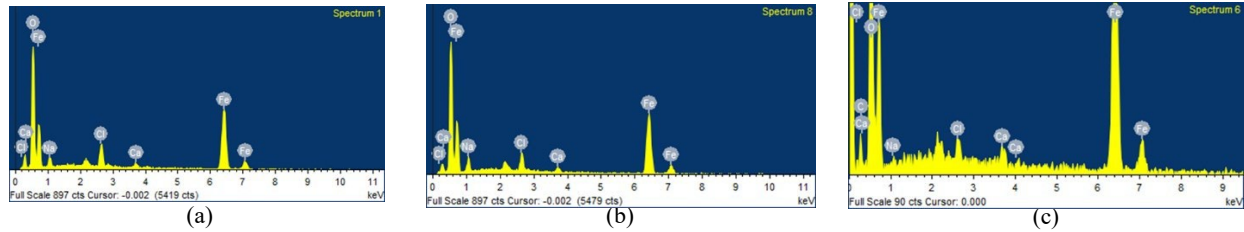


FIGURE 3. EDS Elemental Graph Analysis of 3 parameters samples biofilm; A – 1% (w/v) Sodium Alginate + 0.1 g Iron (III) Oxides, B – 1% (w/v) Sodium Alginate + 0.2 g Iron (III) Oxides, and C – 1% (w/v) Sodium Alginate + 0.3 g Iron (III) Oxides

TABLE 4. EDS Elemental Analysis of Sodium Alginate 1% (w/v) with Iron (III) Oxide Biofilm

Sample Element	A		B		C	
	Weight (%)	Atomic (%)	Weight (%)	Atomic (%)	Weight (%)	Atomic (%)
Fe	59.76	32.21	59.11	31.43	52.36	22.75
O	31.43	59.14	32.19	59.75	31.07	47.11
Na	2.79	3.65	3.61	4.66	0.20	0.21
Ca	1.11	0.83	1.15	0.85	1.00	0.61
Cl	4.90	4.16	3.94	3.30	1.28	0.87

The chemical elemental analysis of EDS for beads can be found in the graph in Figure 4 and in Table 5. The elements' composition was quite different compared to those found in biofilm. Elements that were found in beads were, Fe^{2+} , O^{2-} , and Ca^{2+} . The biofilm and beads for all samples A, B and C should have the exact composition of elements. However, they might have different weight percentages of the elements considering the size and shape of the samples. Both biofilm and beads were prepared from the same source of the solution, but since the differences in the presence of elemental analysis, both biofilm and beads vary. This could be due to the differences in methodological process in which the, for the biofilm, the solutions were cast and soaked into calcium chloride that may have bonded with the solutions while forming into biofilms. In contrary the formation of the beads in which the solutions were dropped into calcium chloride according to the volume in which was influenced by the diameter size of the syringe needle. When the solutions were dropped into calcium chloride, they crosslinked and formed beads. Due to the process, it was possible that not much calcium chloride managed to bond to the S.A./iron (iii) oxide solution.

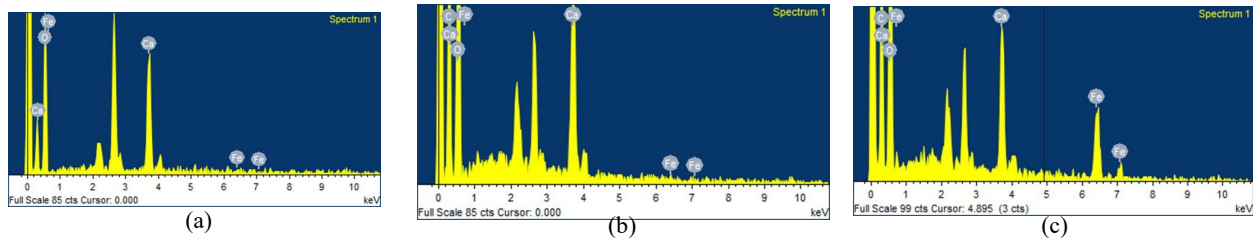


FIGURE 4. EDS Elemental Graph Analysis of 3 parameters samples beads; A – 1% (w/v) Sodium Alginate + 0.1 g Iron (III) Oxides, B – 1% (w/v) Sodium Alginate + 0.2 g Iron (III) Oxides, and C – 1% (w/v) Sodium Alginate + 0.3 g Iron (III) Oxides

TABLE 5. EDS Elemental Analysis of Sodium Alginate 1% (w/v) with Iron (III) Oxide Beads

Sample Element	A		B		C	
	Weight (%)	Atomic (%)	Weight (%)	Atomic (%)	Weight (%)	Atomic (%)
Fe	2.15	0.76	0.49	0.14	16.18	5.15
O	68.24	84.58	20.00	27.04	51.88	57.64
Ca	29.61	14.65	12.92	5.23	9.70	4.30

X-Ray Diffraction (XRD) Analysis

XRD analysis was carried out to determine the chemical characteristic and the presence of crystalline Sodium Alginate incorporated with Iron (III) Oxides. From the XRD Analysis in Figure 5, it was observed that there are eight intense peaks at $2\theta = 22.195^\circ$ (Sodium Iron Oxide), 31.615° (Halite), 31.705° (Sodium Iron Oxide), 35.695° (Magnetite), 45.355° (Iron Oxide), 45.505° (Halite), 62.905° (Maghemite) and at 62.935° (Maghemite). The chemical elemental analysis of EDS for beads is illustrated in the graph in Figure 4 and Table 5. The XRD peak for sample A is slightly broader and less intense as compared to the XRD peak for samples B and C [23]. The difference in the broadness of the XRD peak at $2\theta = 22.195^\circ$ due to the presence of Na phases which indicates the ion exchanges between Na^+ by Fe^{2+} ions making it existed in a larger amorphous phase [23].

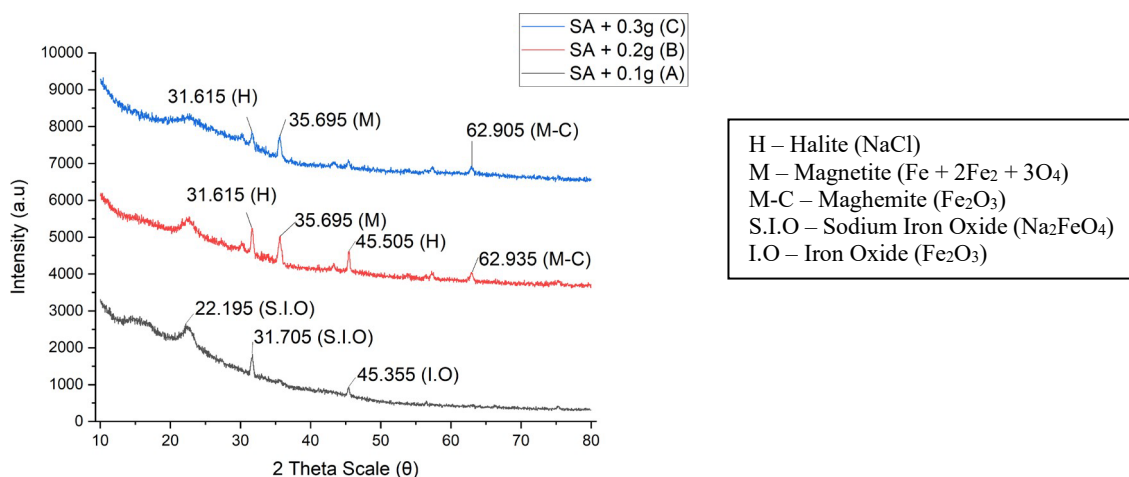


FIGURE 5. XRD Graph Analysis of 3 samples; A – 1% (w/v) Sodium Alginate + 0.1 g Iron (III) Oxides, B – 1% (w/v) Sodium Alginate + 0.2 g Iron (III) Oxides, and C – 1% (w/v) Sodium Alginate + 0.3 g Iron (III) Oxides Biofilm

Atomic Force Microscopy (AFM) Analysis

Based on the 3D AFM images in Figure 6 and surface roughness data tabulated in Table 6, it was observed that all three samples have different values of surface roughness. R_q and R_a values increase as the samples vary in the weight of iron oxides increases. The increase in values shows that in the presence of iron oxides, the interaction of alginate/iron oxides with calcium chloride made it possible to form hills and valley morphologies of roughness. No studies have been undertaken to determine the ideal surface roughness for this application. However, a surface with a higher roughness value is desirable for wound healing and in any biomedical application. High surface roughness increases surface area, which in turn facilitates cell adhesion and proliferation [25]. The samples with the rougher surface which is sample C gave a more desirable result to be used as a wound healing application.

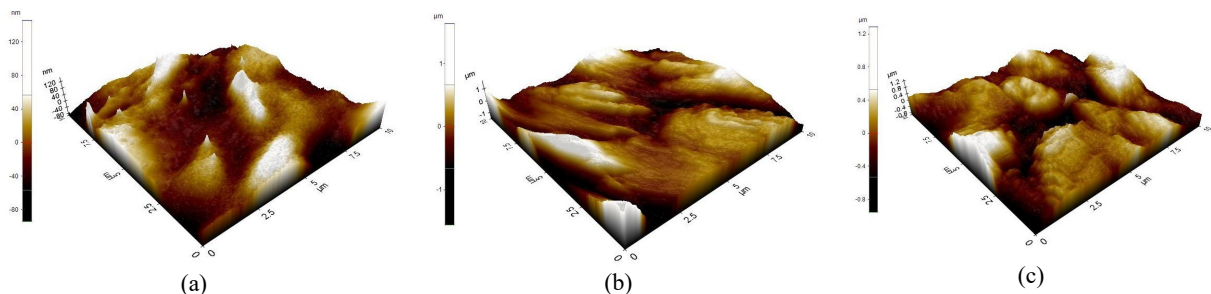


FIGURE 6. 3D AFM Images of 3 parameters samples; A – 1% (w/v) Sodium Alginate + 0.1 g Iron (III) Oxides, B – 1% (w/v) Sodium Alginate + 0.2 g Iron (III) Oxides, and C – 1% (w/v) Sodium Alginate + 0.3 g Iron (III) Oxides

TABLE 6. Roughness Parameters for 1% (w/v) Sodium Alginate with Iron (III) Oxides

Samples	Roughness Parameters		
	Roughness Peak to Valley, Rpv (nm)	Roughness Root Mean Square, Rq (nm)	Roughness Average, Ra (nm)
1% (w/v) + 0.1 g (A)	21.524	4.598	3.708
1% (w/v) + 0.2 g (B)	80.311	19.779	16.373
1% (w/v) + 0.3 g (C)	91.247	21.128	16.909

CONCLUSION

In conclusion, Sodium Alginate incorporated with Iron (III) Oxides was successfully fabricated into biofilm and beads manually using a syringe. The fabricated biofilm and beads varied in the weight of iron oxides used; 0.1 g, 0.2 g, and 0.3 g. Based on the SEM microstructure analysis, it was observed that as the amount of the iron oxides increased in each sample, they became more porous, and grains were present on the surface microstructure of biofilm and beads. From EDS elemental analysis, it was proven to find the elements such as Fe^{2+} , O^{2-} , Na^+ , Ca^{2+} , and Cl^- in biofilm. However, only Fe^{2+} , O^{2-} , and Ca^{2+} were found during EDS analysis in the form of beads which could be due to the formation of the beads. The S.A./Iron (III) Oxide solution was dropped into CaCl_2 solution, which only gives a percentage of chloride ions to be identified from the beads. XRD analysis found intense peaks at $2\theta = 22.195^\circ$, 31.615° , 31.705° , 35.695° , 45.355° , 45.505° , 62.905° , and 62.935° . Lastly, AFM roughness analysis shows that the increment of iron oxide used in the samples forms different hills and valleys on the roughness morphologies of the biofilm, which has made it possible and more desirable to be used as part of the biomedical application which can or may facilitates cell adhesion and proliferation, especially in wound healing application.

ACKNOWLEDGMENTS

The authors would like to thank the Ministry of Higher Education Malaysia for funding this research under the Fundamental Research Grant Scheme (FRGS/1/2018/STG07/UTHM/02/6).

REFERENCES

1. J. A. Sánchez-Fernández, R. D. de León, and R. Cué-Sampedro, "Pharmaceutical and synthetic hormone removal using biopolymer membranes," in *Biopolymer Membranes and Films: Health, Food, Environment and Energy Applications*, edited by M. A. de Moraes, C. F. da Silva, and R. S. Vieira (Elsevier, 2020), pp. 397-421.
2. C. Li, J. Lu, S. Li, Y. Tong, and B. Ye, *Materials* **10**, 84, 1-14 (2017).

3. A. Ahmad, N. M. Mubarak, F. T. Jannat, T. Ashfaq, C. Santulli, M. Rizwan, A. Najda, M. Bin-Jumah, M. M. Abdel-Daim, S. Hussain, S. Ali, [Processes](#) 9(1), 137 (2021).
4. M. S. Hasnain, E. Jameel, B. Mohanta, A. K. Dhara, S. Alkahtani and A. K. Nayak, "Alginates: sources, structures, and properties," in *Alginates in Drug Delivery*, edited by A. K. Nayak and M. S. Hasnain (Academic Press, United Kingdom, 2020), pp. 1-17.
5. F. M. Chen, and X. Liu, "Advancing biomaterials of human origin for tissue engineering," in *Progress in Polymer Science* ,53, edited by G. C. Berry and K. Matyjaszewski (ScienceDirect, USA, 2016), pp 86-168.
6. A. Sood, V. Arora, J. Shah, R. K. Kotnala, and T. K. Jain, [Mater. Sci. Eng. C](#) **80**, 274-281 (2017).
7. A. V. Samrot, C. S. Sahithya, J. S. A, and S. K. Purayil, "A review on synthesis, characterization and potential biological applications of superparamagnetic iron oxide nanoparticles," in *Current Research in Green and Sustainable Chemistry Vol. 4*, edited by A. S. Matharu (Elsevier, UK, 2021), pp 100042.
8. P. M. Bedê, M. H. P. da Silva, A. B. H. da Silva Figueirdo, and P. V. Finotelli, [Polimeros](#) **27**, 267-272 (2017).
9. Z.M. Saiyed, S. D. Telang, and C. N. Ramchand, *BioMag Res Tech* **1**, 2, 1-8 (2003).
10. M. A. Morales, P. V. Finotelli, J. A. H. Coaquira, M. H. M. Rocha-Leão, C. Diaz-Aguila, E. M. Baggio-Saitovitch and A. M. Rossi, [Mater. Sci. Eng. C](#) **28**, 253-257 (2008).
11. S. Bucak, B. Yavuztürk, and A. D. Sezer, "Magnetic Nanoparticles: Synthesis, Surface Modifications and Application in Drug Delivery," in *Recent Advances in Novel Drug Carrier Systems*, edited by A. D. Sezer (Intech, Croatia 2012), pp 165-200
12. C. Lucena-Serrano, A. Lucena-Serrano, A. Díaz, M. Valpuesta, G. Villaverde, J. Manuel López-Romero, F. Sarabia, M. Laurenti, J. Rubio-Retama, and R. Contreras-Cáceres, [Bioorganic Med. Chem.](#) **69**, 116910 (2022).
13. A. Shirangi, F. Mottaghtalab, S. Dinarvand and F. Atyabi, [Int. J. Biol. Macromol.](#) **221**, 604-612 (2022).
14. S. J. Madu, D. Hassan, N. Igbokwe, O. A. Orugun and J. Muazu, "Temperature-sensitive polymers for biomaterials for drug delivery, gene delivery, and tissue engineering," in *Polymeric Biomaterials for Healthcare Applications*, edited by K. Varaprasad (Woodhead Publishing, 2022), pp 335-367.
15. X. Sun, J. Shi, X. Xu, and S. Cao, [Int. J. Biol. Macromol.](#) **59**, 273-281 (2022).
16. P. Li, Y. Dai, J. Zhang, A. Wang and Q. Wei, [Int. J. Biomed. Sci.](#) **4** (3), 221-228 (2008).
17. T. A. Sonia, and C. P. Sharma, [Adv. Polym. Sci.](#) **243**, 23-54 (2011).
18. X. Z. Shu, and K. J. Zhu, [Int. J. Pharm.](#) **201** (1), 51-58 (2000).
19. A. Gonzalez-Pujana, G. Orive, J. L. Pedraz, E. Santos-Vizcaino, and R. M. Hernandez, " Alginate Microcapsules for Drug Delivery," in *Alginates and Their Biomedical Applications*, edited by Bernd H. A. Rehm and M. Fata Moradali (Springer, Singapore, 2018)), pp 67-100.
20. D. T. Nguyen, N. M. Nguyen, D. M. Vu, M. H. Tran, and V. T. Ta, *J Anal Methods Chem*, 5576283 (2021).
21. A. Sosnik, *Int. Sch. Res. Notices Pharm.*, 926157 (2014).
22. Wahajuddin, and S. Arora, [Int. J. Nanomedicine](#), **7**, 3445-3471 (2012).
23. Y. L. Cheryl-Low, K. L. Theam, and H. V. Lee, "Alginate-derived solid acid catalyst for esterification of low-cost palm fatty acid distillate," in *Energy Conversion and Management* 106, (Elsevier, UK, 2015), pp 932-940.
24. P. Decuzzi, B. Godin, T. Tanaka, S. Y. Lee, C. Chiappini, X. Liu, and M. Ferrari, [J. Control. Release](#) **141**, 320-327 (2010).
25. C. M. Srivastava, R. Purwar, R. Kannaujia and D. Sharma, [Fibers Polym](#) **16**, 5, 1020-1030 (2015).